

Classical subharmonic resonances in microwave ionization of lithium Rydberg atoms

Michael W. Noel, W. M. Griffith, and T. F. Gallagher

Department of Physics, University of Virginia, Charlottesville, Virginia 22901

(Received 3 December 1999; revised manuscript received 13 June 2000; published 30 October 2000)

We have studied the ionization of lithium Rydberg atoms by pulsed microwave fields in the regime in which the microwave frequency is equal to or a subharmonic of the classical Kepler frequency of the two-body Coulomb problem. We have observed a series of resonances where the atom is relatively stable against ionization. The resonances are similar to those seen previously in hydrogen, but with significant quantitative differences. We also present measurements of the distribution of states that remain bound after the microwave interaction for initial states near one of the classical subharmonic resonances.

PACS number(s): 32.80.Rm, 42.50.Hz

I. INTRODUCTION

Due to its large size and small binding energy, a Rydberg atom is one of few systems that may be exposed to a well-controlled external field comparable in magnitude to the internal field binding the electron. Experiments have shown that ionization of Rydberg atoms by electric fields is far richer than was anticipated. For example, ionization of hydrogen in a static field is quite different from ionization of other atoms, in which Rydberg electrons are bound by a non-Coulombic potential, although in both cases the passage of the electron over (or tunneling through) the saddle point in the combined atom-Stark potential plays a key role [1]. In contrast, ionization by a field pulse that is short compared to the period of a classical electron's orbit, $2\pi n^3$ for the two-body Coulomb problem, where n is the principal quantum number, occurs by momentum transfer and has little to do with the existence of a saddle point in the potential [2,3]. Ionization by sinusoidal microwave fields combines aspects of ionization by static fields and by half-cycle pulses, and not surprisingly, it also depends on the frequency of the microwave field relative to the Kepler frequency, the frequency of a classical electron's orbit. A convenient way to express the importance of the relative frequencies is to use, rather than the microwave angular frequency ω , the scaled angular frequency $\omega_0 = n_0^3 \omega$, the ratio of the microwave frequency to the Kepler frequency. Not surprisingly, the most interesting regime is that in which $\omega_0 \sim 1$.

The first systematic experimental study in the range $0.2 < \omega_0 < 0.6$ was reported by van Leeuwen *et al.* [4] for the interaction between a hydrogen atom and a few hundred cycle microwave pulse that turned on and off slowly. They examined the onset of ionization as the initial state n_0 was varied, to vary the scaled frequency, and observed a staircase-like behavior in the ionization field versus n . The steps in this staircase were located at the scaled frequencies where the microwave frequency was a subharmonic of the classical frequency; i.e., at $\omega_0 = 1/4, 1/3, 2/5$, and $1/2$. These data have subsequently been analyzed in a number of theoretical reports that have furthered both our classical and quantum-mechanical understanding of the ionization process in this regime [5–12]. In particular, calculations of ionization fields based on one- and two-dimensional classical models

showed remarkable agreement with the observed behavior [13].

In this paper, we present the experimental results of a systematic study of microwave ionization of lithium Rydberg atoms for microwave pulses 5–1100 cycles long in the range of scaled frequency $0.2 < \omega_0 < 1.5$. We have observed a series of stairsteps in the ionization thresholds as a function of the initial state, which are similar to those observed in hydrogen. However, there are significant differences in the details of our curves compared to those previously reported for hydrogen. In addition to the threshold fields for ionization, we have measured the final-state distributions for the atoms not ionized by the microwave pulse. These measurements show that near the stairsteps in the ionization field, which occur at subharmonic resonances, the atoms are left in the same final states, suggesting that the electron's classical motion may be pulled into resonance with the applied microwave field.

The classical parameters used above are derived from the two-body Coulomb problem. For a nonhydrogenic atom, the Rydberg electron orbits a finite-size core, which causes the axis of the classical orbit to precess [14]. The more complicated dynamics in this case brings into question the utility of scaling by the classical Kepler frequency. In some cases a scaling that is more closely related to the precessional frequency may be more appropriate [15]. For the experiment presented here we used nearly hydrogenic $np, |m|=1$ states of lithium, which have a quantum defect of 0.05. Since the effects of the Li^+ core have been minimized by this choice of state, we have chosen to scale by the classical Kepler frequency in our discussion and analysis of this experiment.

II. EXPERIMENT

This section begins with a brief description of our experiment followed by detailed descriptions of the individual components involved. First, a Rydberg state of lithium was prepared using a combination of dye laser pulses. Next, the atoms were exposed to an 11.5-GHz microwave pulse. Finally, a slowly rising electric field was applied that ionized atoms that remained bound after the microwave interaction. The number of electrons from field ionization was measured (we call this the remaining atom signal) as the microwave amplitude was varied, which revealed a sharp threshold for

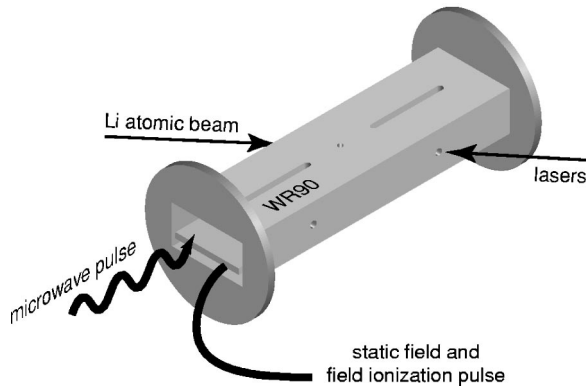


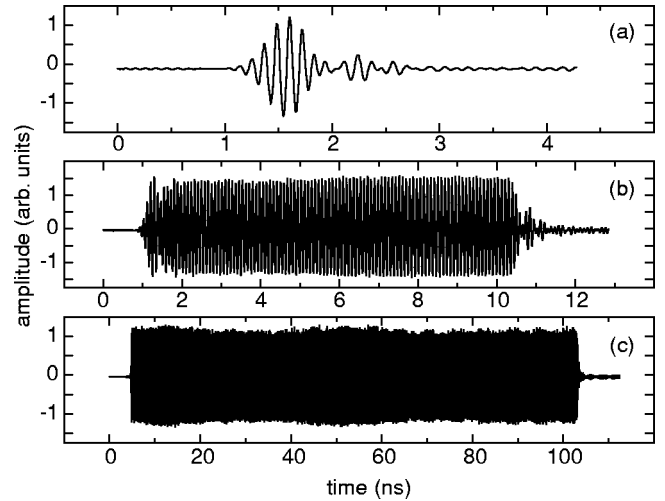
FIG. 1. Waveguide region in which our experiment took place.

ionization. By measuring such ionization thresholds for initial Rydberg states in the range $47 < n_0 < 95$, we obtained information about the process of microwave ionization in the region of the classical subharmonic resonances.

Our experiment took place inside a piece of WR90 waveguide as shown in Fig. 1. Lithium atoms from an effusive source entered the waveguide through a small hole in one of its sides. The three dye laser beams used to excite the Rydberg state entered the waveguide through a small hole on the opposite side. The microwave power was transmitted through the waveguide in the TE_{10} mode. A copper septum, to which we applied the field ionization pulse, was placed inside the waveguide just below the atom and laser beams. The electrons resulting from field ionization were accelerated through a small hole in the top of the waveguide and onto a dual microchannel plate detector.

Three nanosecond pulsed dye lasers excited the lithium Rydberg atoms through the $2s \rightarrow 2p$, $2p \rightarrow 3s$, and $3s \rightarrow np$ transitions. The first two lasers were built in the standard Littman configuration [16] and operated at wavelengths of 671 nm and 813 nm, respectively. For the third transition to the Rydberg state we used a dual grating Littman style laser operating near 617 nm [17]. This laser had a bandwidth of ~ 4 GHz that was sufficient to selectively excite single Rydberg states as high as $n \approx 100$. The polarization of this laser was orthogonal to that of the microwave field in order to excite $|m|=1$ states.

The three microwave pulses used in this experiment, shown in Fig. 2, were formed in the following way. The continuous wave output of a Hewlett Packard microwave sweep oscillator running at 11.5 GHz was sent into the local oscillator port of a mixer. Into the intermediate frequency port of the mixer we sent a voltage step with a fast rising edge (~ 100 ps). This produced, at the radio frequency port of the mixer, a microwave field that turned on quickly. This signal was fed into a second mixer and combined with a fast falling voltage step to form the fast microwave pulse. The remaining microwave field outside the desired window defined by the fast edges was further reduced by mixing the fast microwave pulse with a square voltage pulse with rise and fall times of ~ 1 ns and duration slightly longer than the microwave pulse. The microwave pulse was then preamplified in two stages. After preamplification, the pulse passed through a fast microwave switch that was gated open for a

FIG. 2. Three microwave pulses used in our experiment of durations (a) $\sim 1/2$ ns, (b) ~ 10 ns, and (c) ~ 100 ns.

time slightly longer than the microwave pulse. The switch had a rise and fall time of 10 ns and a contrast ratio of 80 dB and served to eliminate any broad band noise generated during preamplification that was outside the pulse window. Finally, the microwave pulse was amplified to ~ 20 W in a pulsed traveling wave tube amplifier, which was gated on for 300 ns.

The amplified pulse passed through a voltage-controlled attenuator with an attenuation range of 40 dB. Using a coaxial line, it was fed into the vacuum chamber where it was coupled into the waveguide. At the other end of the waveguide the pulse was coupled out into another coaxial line, which passed out of the vacuum system where the pulse was attenuated and monitored on a sampling oscilloscope. After being amplified and traveling through the entire microwave circuit, the rise and fall times of the pulse were lengthened somewhat (~ 3 cycles or 270 ps), as seen in Fig. 2. There was also a glitch about $1/2$ ns after the beginning and end of the pulse due to a reflection in the microwave circuit that we were not able to eliminate. The peak power in the microwave pulse was calibrated using a Hewlett Packard 432A power meter and converted to a field amplitude using the known geometry of the waveguide interaction region. We estimate a microwave field uncertainty of $\pm 10\%$.

The phase of the microwave carrier wave was also locked to the pulse envelope. This was accomplished using an arbitrary waveform generator that produced three signals; a 250-MHz sinusoidal wave, a rising voltage step, and a falling voltage step. The phases of these three signals were locked to the 1-GHz clock of the generator. The 250-MHz signal was fed into a comb generator whose output was mixed with a portion of the continuous wave output of the sweep oscillator. The output from the intermediate frequency port of this mixer was sent through a low pass filter and fed into the frequency modulation input of the sweep oscillator. This locked the 11.5 GHz-output of the microwave oscillator to the 46th harmonic of the 250-MHz signal and consequently, to the voltage steps that were used to form the leading and trailing edges of the pulse.

The field ionization pulse was applied to the septum in the waveguide approximately 300 ns after the microwave pulse, producing a pulse that rose to 450 V/cm in 1 μ s. We also applied a constant voltage to the septum to minimize stray fields so that the atoms were in nearly zero electric field during the microwave interaction. The field was minimized by tuning the Rydberg laser to an energy midway between the $80p$ and $81p$ states. With the polarization of the laser rotated to be aligned with the electric field axis, we then scanned the voltage applied to the septum. When the field seen by the atoms was not zero, the laser could populate the $81s$ state that lies approximately midway between the neighboring p states. Thus the field was minimized by adjusting the voltage to minimize the $81s$ -state population. We estimate a residual field of less than 50 mV/cm using this technique. The residual field determines the highest principal quantum number that is stable against field ionization, sometimes termed n cutoff and denoted n_c . Our residual field of 50 mV/cm leads to $n_c = 280$.

III. IONIZATION THRESHOLDS

Figure 3 shows several typical ionization threshold measurements. We measure the total number of electrons that remain bound to the atom after interaction with the microwave pulse. When normalized to the total number of atoms initially excited to the Rydberg state, this signal is simply the complement of the ionization probability. We characterize the ionization threshold by three fields, the fields at which 10%, 50%, and 90% of the atoms are ionized. These three ionization levels are plotted as a function of the initial state excited in Fig. 4 for the interaction with microwave pulses of 1/2-ns, 10-ns, and 100-ns, durations. In general, the threshold fields decrease in a series of stairsteps with the flat portions of the steps lying at the locations of the classical subharmonic resonances. In other words, all initial states near a classical subharmonic resonance ionize at essentially the same field amplitude. In some cases the threshold fields actually increase slightly as we pass through one of the resonances.

Some deviations from this general behavior are also seen. The curve for 90% ionization in Fig. 4(a) (1/2-ns microwave pulse) is nearly flat for $n_0 > 65$. The lack of n dependence is in part due to the excitation of population to extremely highly excited states during the microwave interaction [18]. Due to the long Kepler orbit time of these extremely highly excited states, these electrons do not return to the core during the short microwave pulse and can remain bound even for very large field amplitudes. A second deviation from the general stairstep behavior is seen in the 10% ionization curve of Fig. 4(c) (100-ns microwave pulse). The threshold fields seem to vary erratically for low n_0 , and for the lowest initial states the field required to begin ionizing is quite low, ~ 5 V/cm for $n_0 = 50$. In this case the ionization curve shows a double threshold [Fig. 3(a)] that is actually a signature of the nonhydrogenic nature of our atom. This field is about $1/3n_0^5$ (in atomic units), which is the field at which Stark states from neighboring manifolds cross. Due to the finite size of the Li^+ core, the Stark states do not actually

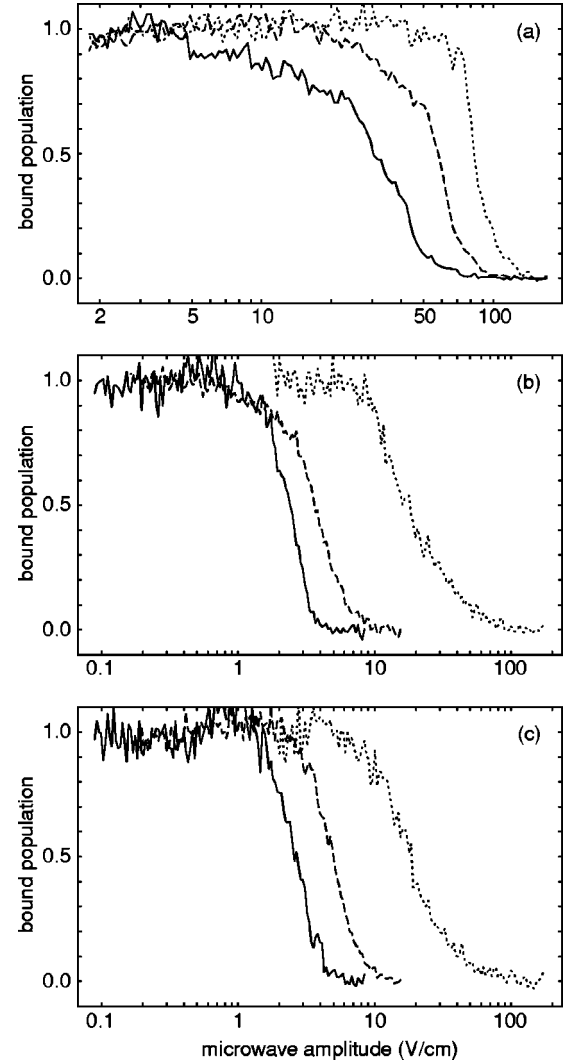


FIG. 3. Microwave ionization thresholds for (a) $n_0 = 50$, (b) $n_0 = 80$, and (c) $n_0 = 90$ interacting with 1/2-ns (dotted curves), 10-ns (dashed curves), and 100-ns (solid curves) microwave pulses.

cross, but exhibit small avoided crossings [19] due to the core-induced couplings, which allow a ladder climbing mechanism to produce ionization at these low fields [20,21]. For lithium $|m| = 1$ states the avoided crossings between Stark states are small, leading to a small probability of making the transitions necessary for ladder climbing as each field cycle sweeps through the avoided crossings at $1/3n^5$. Consequently, we only observe these low thresholds for the longest pulses, which sweep through the avoided crossings many times, and for the lowest initial states, where the avoided crossings are largest. The precise form and amplitude of the $1/3n_0^5$ ionization feature is determined by microwave multiphoton resonances, leading to the apparent erratic variation of the 10% ionization thresholds of Fig. 4(c) [22,23]. For microwave pulses 10-ns long and shorter the lithium states we have studied appear to be similar to their hydrogen analogues.

The ionization thresholds of hydrogen also show structure or “subthreshold peaks” in some cases [24]. This structure is attributed to avoided crossings between Floquet states (states of the atom dressed by the microwave field) [25–27].

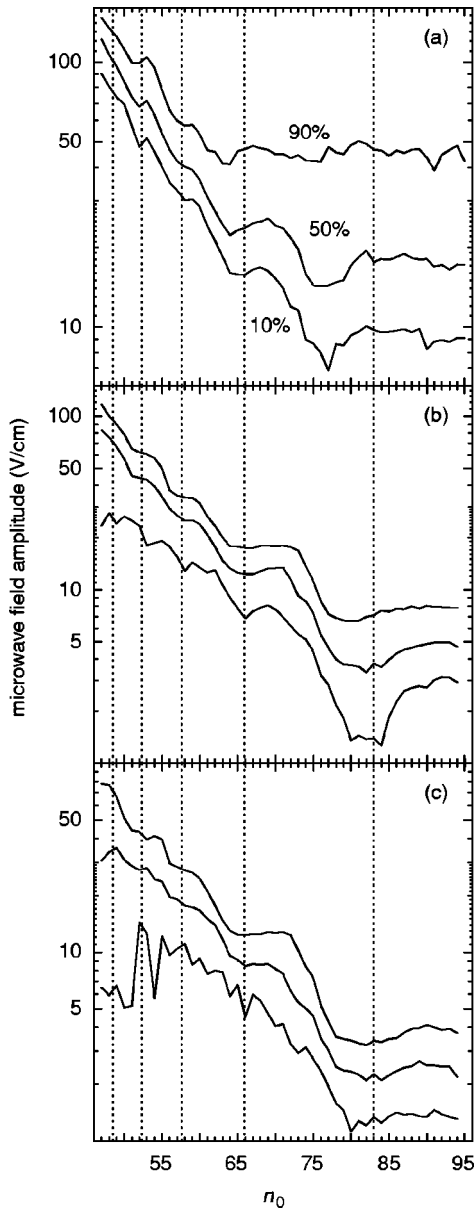


FIG. 4. Threshold fields required for 10%, 50%, and 90% ionization plotted versus the initial state excited for the interactions with (a) 1/2-ns, (b) 10-ns, and (c) 100-ns pulses. The dotted vertical lines are at the $\omega_0 = 1/5$, $1/4$, $1/3$, $1/2$, and 1 subharmonic resonances.

This theory predicts a series of sharp spikes in the ionization level as the field is swept through avoided crossings between Floquet states. These sharp spikes are smoothed out in the experimental curves, but where they were densely clustered subthreshold peaks appear. Avoided crossings between Floquet states may also be sufficient to account for the structure seen in Fig. 3 for lithium [15]. In fact, multiphoton resonances are also important in the ladder climbing mechanism described earlier, and for alkali atoms there is a close connection between these resonances and multiple traversals of the Stark-state avoided crossings at $1/3n^5$ [22].

Some structure in the ionization threshold curves for higher initial states is also apparent, e.g., the shoulder on the

curve in Fig. 3(b) for ionization of $n_0 = 80$ with a 10-ns pulse. In this regime the core-induced Stark state avoided crossings, upon which the ladder climbing mechanism relies, are traversed very rapidly on each cycle of the microwave field, making this an unlikely explanation for the observed structure, especially since the pulse is only 110 cycles long. A hydrogenic Floquet model may be sufficient for understanding most of the behavior in this regime. A more detailed comparison of our experimental results and those obtained for hydrogen is given in Sec. V.

IV. STATE DISTRIBUTIONS

Outside of the two deviations described in Sec. III, the staircase behavior of the ionization thresholds dominates Fig. 4. In order to gain insight into the origin of these steps, we have measured the distribution of states in which the remaining atoms are left after the microwave pulse using selective field ionization. After the microwave interaction, we apply a slowly rising electric field pulse. Electrons bound in high n states ionize in a small electric field early in the field ionization pulse while those bound in low n states require a larger field to ionize and thus ionize at a later time. By collecting the time-resolved electron signal, we obtain a record of the final bound-state distribution.

Figure 5 shows a calibration scan of the arrival time of the electron versus principal quantum number. In this scan, the microwave pulse was off and the final laser was tuned through the Rydberg series as we collected the time-resolved electron signal on a digital oscilloscope. We create an image of these data by mapping the electron signal to a gray scale with black representing a large signal, and white, no signal. The horizontal axis is the arrival time of the electron at the detector, and the vertical axis is the laser frequency. As the laser is tuned to higher n states, the peak in the electron signal moves to earlier times. Near $n = 55$ there is a double-peaked structure in the time-resolved electron signal, which is due to two pathways for field ionization of the electron [28]. At low n , the anticrossings between Stark states are large relative to their size at high n . Since the rise time of the field ionization pulse does not change, ionization of low n states proceeds adiabatically while high n states are ionized diabatically. Adiabatic field ionization occurs at a lower field value than diabatic ionization resulting in an earlier arrival time of the adiabatic electron signal. For intermediate values of n , we see both adiabatic and diabatic components in the field ionization signal.

In an effort to understand the flat steps seen in Fig. 4, we plot in Fig. 6(a) the final state distributions as a function of field amplitude for a series of initial states of principal quantum number n_0 near $n_0 = 66$ for the interaction with a 1/2-ns pulse. Again, the electron signal is mapped to a gray scale. The vertical axis in these images is now microwave amplitude while the horizontal axis is the arrival time of the electron. For the horizontal axis we use the diabatic calibration from Fig. 5 since this ionization pathway dominates at these values of n . In each of these images we see that at low power (top of each image) all of the population resides in the initial state. As the field is increased, population spreads out to

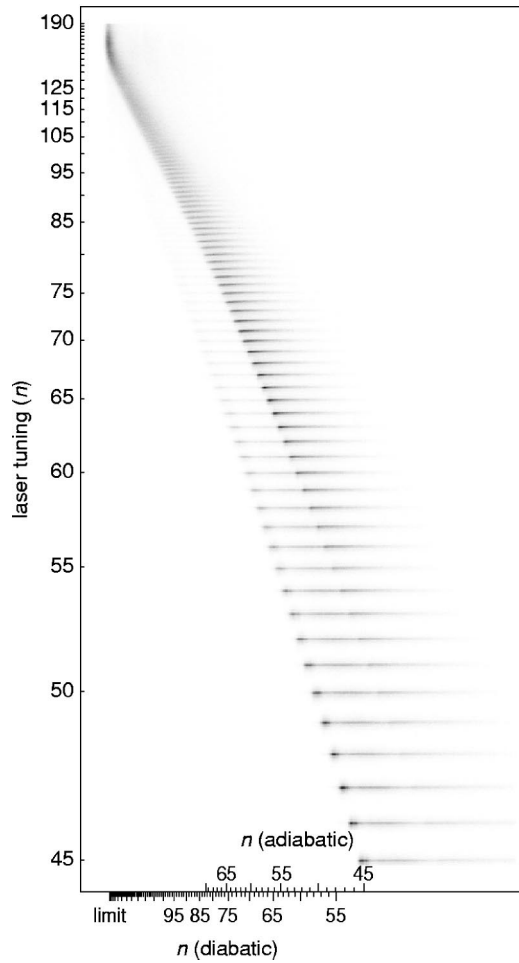


FIG. 5. Calibration scan for the time-resolved electron signal. The electron signal is mapped to a gray scale with black corresponding to large signal and white to no signal. In this image the laser tuning increases along the vertical axis and the electron arrival time increases along the horizontal axis. The peak positions of both the diabatic and adiabatic field ionization signals are marked on the bottom axis.

neighboring states. At the highest field amplitude everything is ionized and there is no bound-state signal left. The ionization threshold shown in Fig. 3 is simply the gated integration of the associated time-resolved signal. In each of the images of Fig. 6, some population accumulates at the point marked “limit” as the field increases. These are electrons bound in the extremely highly excited states discussed earlier. Here we focus our attention on the redistribution of population to states near the initial state. As shown by Fig. 6(a), at $n_0 = 66$ the population spreads fairly uniformly about the initial state as the field is increased before being ionized. For $n_0 = 64$, the population moves to higher n states just before ionizing. Conversely, at $n_0 = 70$ the electron is pulled to lower n states before ionizing.

A more quantitative measure of this effect is seen in Fig. 6(b). Here we plot the state distributions at 10% ionization for the same series of initial states. At 10% ionization the state distributions for $65 < n_0 < 70$ look nearly identical, and are centered near $n = 66$, which is why all of these states

ionize at nearly the same field, producing the flat spot seen in Fig. 4 near $n_0 = 66$.

Figure 7 shows very similar behavior of the state distribution for ionization with a 10-ns pulse. Again for $65 < n_0 < 70$ the state distributions at 10% ionization are nearly identical, but they appear to be centered near $n = 64$. This apparent shift of the center of the distribution is most likely because population has been distributed among high angular momentum states that ionize at slightly higher fields. The correspondence between n and the ionization field (Fig. 5), is done with np states. Outside this range of initial states the final state distribution at 10% ionization makes an abrupt jump away from the resonance at $n = 66$. For instance, at $n_0 = 72$ the state distribution at 10% ionization is centered near $n = 70$, which in turn leads to a large shift in the ionization threshold.

V. DISCUSSION

We conclude with a comparison between our experimental results and those obtained previously for hydrogen. Our threshold data for lithium ionization by 1/2-ns, 10-ns and 100-ns microwave pulses are replotted in Fig. 8 using classically scaled units. The scaled frequency $\omega_0 = n_0^3 \omega$ was discussed earlier and the scaled field $F_0 = F n_0^4$ (in atomic units), is the microwave field amplitude F scaled by the Coulomb binding field of the initial state $1/n_0^4$. The steps seen in the unscaled representation of this data become sharp peaks in the scaled plots. This scaled representation of the threshold fields facilitates a direct comparison between sets of data taken at different microwave frequencies and for different ranges of initial states. In Fig. 9, we compare our lithium threshold data to the experimental results reported for hydrogen [5]. We make this comparison with our 10-ns (110 cycle) pulses since this comes closest to matching the 300-cycle interaction time used in the hydrogen experiment.

Qualitatively, the results shown in Fig. 9(a) are similar; there is a series of peaks where the atom is more stable against ionization. However, there are many significant quantitative differences. The most obvious of these differences is the overall shift in the positions of the peaks to higher values of the scaled frequency for lithium. There also seems to be less overall structure in the lithium threshold curves; the peaks are quite smooth. While the 10% ionization fields for lithium and hydrogen are nearly the same for $\omega_0 > 1/2$, the lithium fields for 10% ionization fall far below the hydrogen fields at low scaled frequencies, indicating that it is much easier to begin ionizing lithium atoms than hydrogen atoms in this region. Figure 9(b) shows that the 90% ionization fields for lithium and hydrogen are similar at high scaled frequency, but the lithium 90% ionization fields are still somewhat lower than the hydrogenic fields at low scaled frequencies. Apparently the difference between lithium and hydrogen becomes smaller when higher fractional ionization is required. The differences seen in the lithium and hydrogen threshold data stem from the differences in the two experiments. The most obvious and important difference is the atoms used in the experiments.

First, lithium and hydrogen are not the same. Lithium has

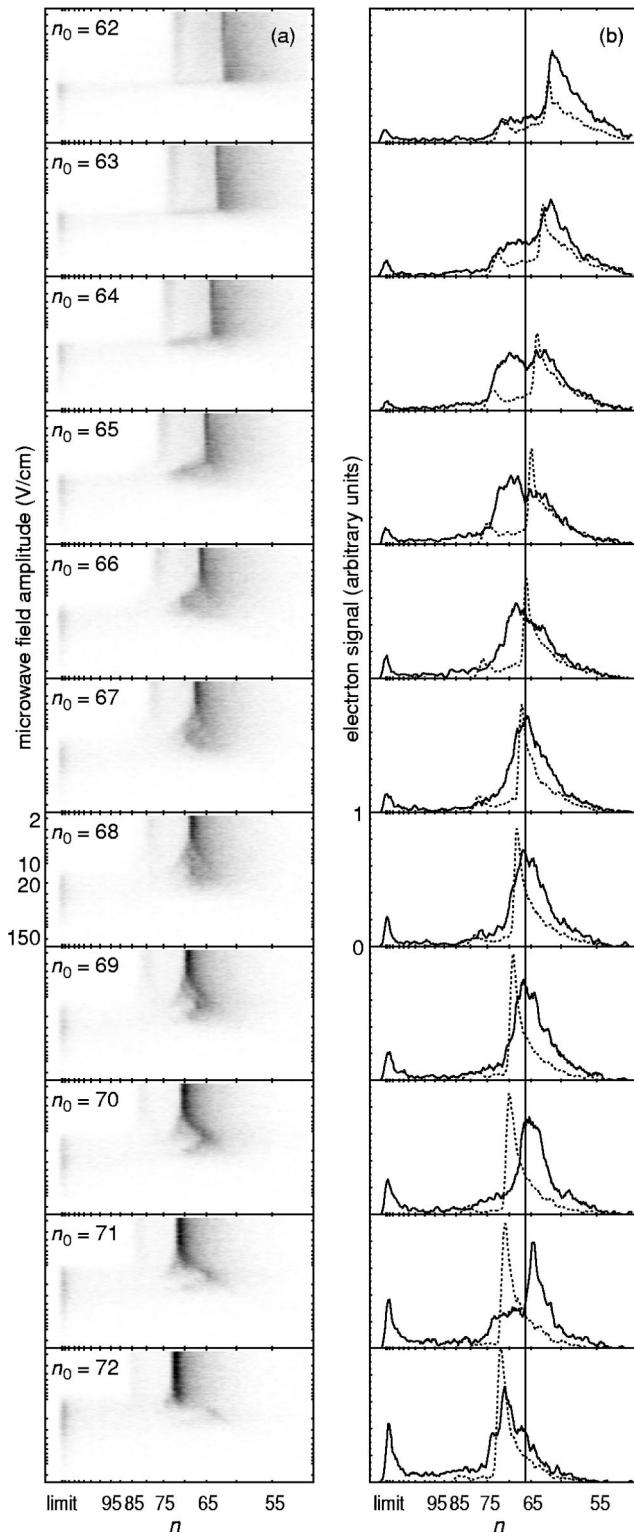


FIG. 6. State distributions as a function of field strength for interaction with a 1/2-ns pulse for initial states near $\omega_0=1/2$. In the first column (a) the time-resolved electron signals are mapped to a gray scale with black corresponding to large signal and white to no signal. In the second column (b) we show lines out of the images in (a) for the time-resolved electron signals at 10% ionization (solid curves) and time-resolved electron signals for the initial states (dotted curves) for the same series of initial limits.

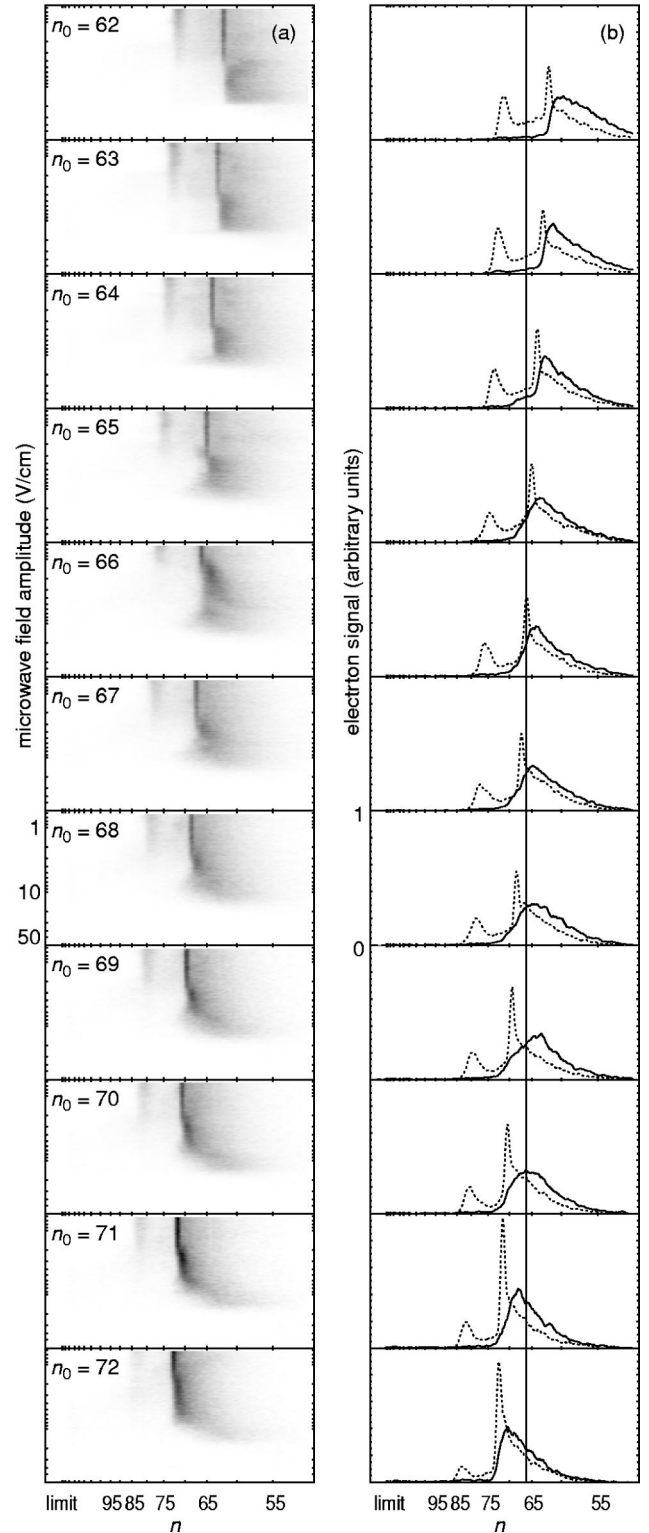


FIG. 7. (a) State distributions as a function of field strength for interaction with a 10-ns pulse for initial states near $\omega_0=1/2$. (b) State distributions at 10% ionization.

a finite-sized core, an effect which we attempted to minimize by using $|m|=1$ states. The largest quantum defect of the $|m|=1$ levels is that of the p states, $\delta_p=0.05$. A second significant difference in the atoms is that we start with the

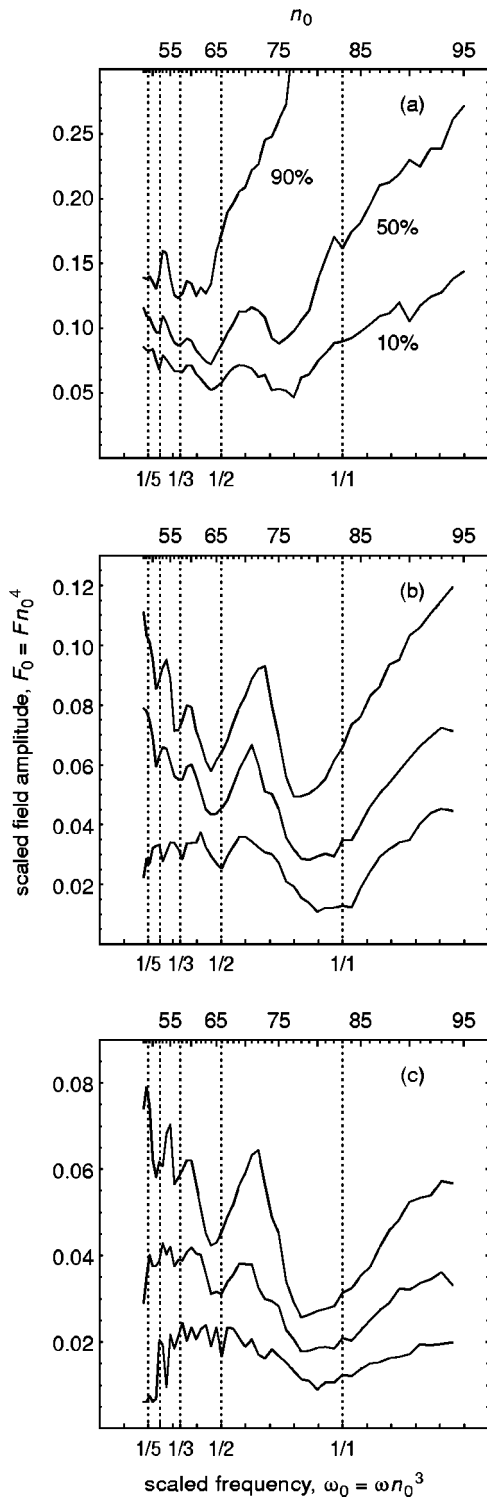


FIG. 8. Threshold fields for 10%, 50%, and 90% ionization plotted in classically scaled units for interaction with (a) 1/2-ns, (b) 10-ns, and (c) 100-ns pulses.

Rydberg atoms in lithium np states, while in the hydrogen experiments they are in a mixture of lm states. We attribute the major observed differences, the location of the resonances and the overall field strengths required, to these two sources. Why the resonances are shifted in lithium relative to hydrogen is not obvious, but the fact that the ionization fields

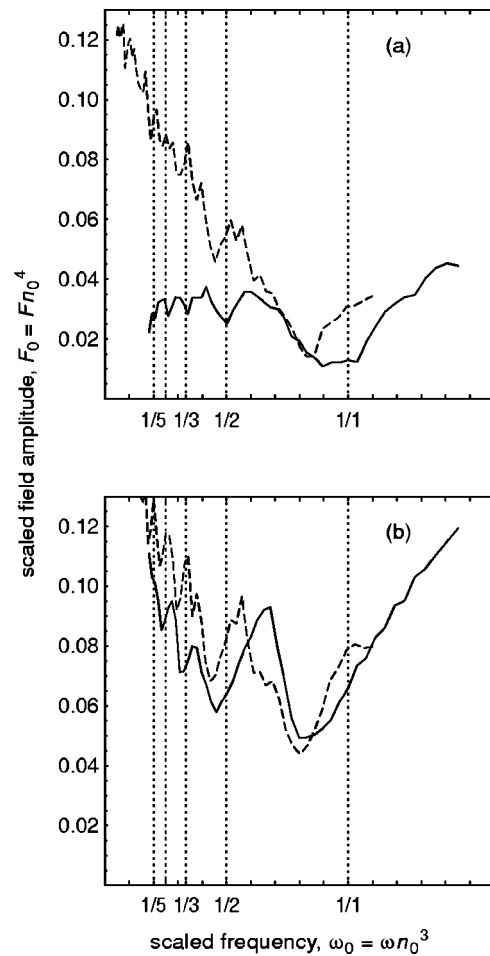


FIG. 9. Comparison in scaled units of our threshold curves for lithium Rydberg atoms interacting with a 10-ns pulse (solid curves) and threshold curves for hydrogen (dashed curves) [from P. M. Koch and K. A. H. van Leeuwen, Phys. Rep. 255, 289 (1995)] for (a) 10% and (b) 90% ionization.

are lower for lithium, especially for low n , is likely due to the n changing, or ladder climbing, transitions, a possibility that does not exist in hydrogen. At higher scaled frequencies our thresholds come closer to matching those for hydrogen, indicating a more hydrogenic behavior of the lithium states in this regime.

The most significant difference in experimental procedure is the fast rise and fall time of our microwave pulse (~ 3 cycles for our experiment compared to ~ 80 cycles for the hydrogen experiment). The effect of the pulse rise and fall time on the classical electron dynamics has been discussed by Jensen and co-workers [6,10,12]. Using a one-dimensional classical model of the hydrogen atom, they have found remarkable agreement between the experimental curves for 10% ionization of hydrogen and the onset of chaotic ionization in the classical system. Justification for the validity of the reduced dimensionality of this model comes from the observation that in a three-dimensional system the highly eccentric orbits that are aligned with the field are easiest to ionize [29,30]. Therefore, using this reduced set of elongated orbits, or equivalently, a one-dimensional model, should be adequate for predicting the onset of ionization.

Using phase-space portraits to display the classical dynamics, they observe stable islands where orbits can be trapped in an otherwise chaotic region of phase space. In this one-dimensional classical model, they find that the stability of the orbits near these islands depends critically on the turn on of the microwave field. For a sudden turn on their theory predicts that the peaks in the ionization threshold curves will flatten out and the thresholds will in general be at lower field amplitudes. While the overall thresholds in our 10% ionization data [Fig. 9(a)] are lower than the hydrogen data, the peaks are still clear. For higher levels of ionization, the peaks in our experimental data become even more pronounced, however, for the reasons stated earlier the one-dimensional model has not been used to predict thresholds for higher levels of ionization.

The effect of pulse rise and fall times has also been investigated using quantum Floquet models [25,31,32]. Although the specific conditions of our experiment have not been addressed, the models indicate a remarkable insensitivity to switching time of the microwave pulse. Even for the extreme case of a square pulse envelope, the atomic response is nearly identical to slower switching times as long as the phase of the microwave field is that of a sine wave at switch on and off. This similarity of a square pulse of sine waves to a slowly turned on pulse has also been shown experimentally for multiphoton transitions between bound states [33].

A second difference is the much higher value of n cutoff in our experiment ($n_c = 280$ for our data versus $n_c = 90$ for the hydrogen data). The effect of our very large n cutoff is most dramatic in the short pulse data. For high n_0 initial states a large amount of population is transferred to extremely highly excited states with $n > 120$. At a level of 90% ionization nearly all of the remaining population is in these states, leading to the very steep rise of this curve in Fig. 8(a). For a 10-ns microwave interaction the maximum transfer of population to states with $n > 120$ is about 3% for the highest initial states. The low n cutoff of the hydrogen experiments has the largest effect as n_0 approaches n_c . It has been shown

that increasing n_c raises the threshold values slightly for large n_0 in the hydrogen experiment [5]. Therefore, the large difference in n_c used in our experiment compared to the hydrogen experiment should only affect the comparison in Fig. 9 for the highest n_0 's, and there the effect should be small.

Examination of the final-state distributions of the remaining bound atoms has received much less attention than the ionization fields. Both experimental [34,35] and theoretical [10] reports of the final-state distributions explore only a few isolated areas of this vast parameter space. The data shown in Figs. 6 and 7 provide complete coverage of the regime $0.01 < F_0 < 0.4$ and $0.42 < \omega_0 < 0.65$ for two pulse widths. These data provide additional insight into the behavior of the ionization threshold curves seen near $\omega_0 = 1/2$. In essence, all initial states near $\omega_0 = 1/2$ ionize at nearly the same field because the population from any of these states is pulled by the field into a nearly identical state distribution centered around the classical subharmonic resonance. This observation supports a suggestion of Buchleitner and Delande regarding the origin of the observed resonance in the ionization threshold field [36]. Specifically, at one of the classical resonances the classical electron's orbit can become phase locked to the microwave field and be quite stable if the phase is such that the electron is near the ion core at the peak of the field. There is some similarity to an electron's orbit in a synchrotron. Quantum mechanically, such a state corresponds to the formation of a wave packet. While our data tell us nothing about the phases of the observed states, they do demonstrate that at the classical resonances the final states are indeed the ones required to form a wave packet that is synchronized with the microwave field.

ACKNOWLEDGMENTS

This work was supported by the Air Force Office of Scientific Research and the National Science Foundation. We thank Lung Ko and P. M. Koch for useful discussions.

-
- [1] Michael G. Littman, Michael M. Kash, and Daniel Kleppner, *Phys. Rev. Lett.* **41**, 103 (1978).
 - [2] R.R. Jones, D. You, and P.H. Bucksbaum, *Phys. Rev. Lett.* **70**, 1236 (1993).
 - [3] Carlos O. Reinhold, Michael Melles, Hai Shao, and Joachim Burgdörfer, *J. Phys. B* **26**, L659 (1993).
 - [4] K.A.H. van Leeuwen, G.V. Oppen, S. Renwick, J.B. Bowlin, P.M. Koch, R.V. Jensen, O. Rath, D. Richards, and J.G. Leopold, *Phys. Rev. Lett.* **55**, 2231 (1985).
 - [5] P.M. Koch and K.A.H. van Leeuwen, *Phys. Rep.* **255**, 289 (1995).
 - [6] R.V. Jensen, *Phys. Scr.* **35**, 668 (1987).
 - [7] V. Gontis and B. Kaulakys, *J. Phys. B* **20**, 5051 (1987).
 - [8] R. Blümel and U. Smilansky, *Phys. Rev. Lett.* **58**, 2531 (1987).
 - [9] R.V. Jensen, M.M. Sanders, M. Saraceno, and B. Sundaram, *Phys. Rev. Lett.* **63**, 2771 (1989).
 - [10] R.V. Jensen, S.M. Susskind, and M.M. Sanders, *Phys. Rep.* **201**, 1 (1991).
 - [11] Bala Sundaram and R.V. Jensen, *Phys. Rev. A* **51**, 4018 (1995).
 - [12] M.M. Sanders and R.V. Jensen, *Am. J. Phys.* **64**, 21 (1996).
 - [13] D. Richards, in *Classical Dynamics in Atomic and Molecular Physics*, edited by T. Grozdanov, P. Grujić, and P. Krstić (World Scientific, Singapore, 1988), p. 269.
 - [14] T.P. Hezel, C.E. Burkhardt, M. Ciocca, L-W. He, and J.J. Leventhal, *Am. J. Phys.* **60**, 329 (1992).
 - [15] Oliver Benson, Andreas Buchleitner, Georg Raitel, Markus Arndt, Rosario N. Mantegna, and Herbert Walther, *Phys. Rev. A* **51**, 4862 (1995).
 - [16] Michael G. Littman and Harold J. Metcalf, *Appl. Opt.* **17**, 2224 (1978).
 - [17] M.G. Littman, *Opt. Lett.* **3**, 128 (1978).
 - [18] Michael W. Noel, W.M. Griffith, and T.F. Gallagher, *Phys. Rev. Lett.* **83**, 1747 (1999).
 - [19] Myron L. Zimmerman, Michael G. Littman, Michael M. Kash,

- and Daniel Kleppner, *Phys. Rev. A* **20**, 2251 (1979).
- [20] P. Pillet, W.W. Smith, R. Kachru, N.H. Tran, and T.F. Gallagher, *Phys. Rev. Lett.* **50**, 1042 (1983).
- [21] P. Pillet, H.B. van Linden van den Heuvell, W.W. Smith, R. Kachru, N.H. Tran, and T.F. Gallagher, *Phys. Rev. A* **30**, 280 (1984).
- [22] R.C. Stoneman, D.S. Thomson, and T.F. Gallagher, *Phys. Rev. A* **37**, 1527 (1988).
- [23] C.R. Mahon, J.L. Dexter, P. Pillet, and T.F. Gallagher, *Phys. Rev. A* **44**, 1859 (1991).
- [24] D. Richards, J.G. Leopold, P.M. Koch, E.J. Galvez, K.A.H. van Leeuwen, L. Moorman, B.E. Sauer, and R.V. Jensen, *J. Phys. B* **22**, 1307 (1989).
- [25] R. Blümel and U. Smilansky, *J. Opt. Soc. Am. B* **7**, 664 (1990).
- [26] Andreas Buchleitner, Dominique Delande, and Jean-Claude Gay, *J. Opt. Soc. Am. B* **12**, 505 (1995).
- [27] Andreas Buchleitner and Dominique Delande, *Chaos, Solitons Fractals* **5**, 1125 (1995).
- [28] T.H. Jeys, G.W. Foltz, K.A. Smith, E.J. Beiting, F.G. Kellert, F.B. Dunning, and R.F. Stebbings, *Phys. Rev. Lett.* **44**, 390 (1980).
- [29] Andreas Buchleitner and Dominique Delande, *Phys. Rev. A* **55**, 1585 (1997).
- [30] A. Krug and A. Buchleitner, *Europhys. Lett.* **49**, 176 (2000).
- [31] R. Blümel and U. Smilansky, *Z. Phys. D: At., Mol. Clusters* **6**, 83 (1987).
- [32] H.P. Breuer, K. Dietz, and M. Holthaus, *Z. Phys. D: At., Mol. Clusters* **8**, 349 (1988).
- [33] W.M. Griffith, Michael W. Noel, and T.F. Gallagher, *Phys. Rev. A* **57**, 3698 (1998).
- [34] James E. Bayfield and David W. Sokol, *Phys. Rev. Lett.* **61**, 2007 (1988).
- [35] R. Blümel, A. Buchleitner, R. Graham, L. Sirko, U. Smilansky, and H. Walther, *Phys. Rev. A* **44**, 4521 (1991).
- [36] Andreas Buchleitner and Dominique Delande, *Phys. Rev. Lett.* **75**, 1487 (1995).